Kirigami-inspired triboelectric nanogenerator as ultra-wide-band vibrational energy harvester and self-powered acceleration sensor

Qi, Youchao; Kuang, Yang; Liu, Yaoyao; Liu, Guoxu; Zeng, Jianhua; Zhao, Junqing

Published in:
Applied Energy

DOI:
10.1016/j.apenergy.2022.120092

Publication date:
2022

Kirigami-Inspired Triboelectric Nanogenerator as Ultra-Wide-Band Vibrational Energy Harvester and Self-Powered Acceleration Sensor

Youchao Qi [a, c, 1], Yang Kuang [b, 1], Yaoyao Liu [a, c], Guoxu Liu [a, c], Jianhua Zeng [d], Junqing Zhao [a, c], Lu Wang [e], Meiling Zhu [b, *], Chi Zhang [a, c, d, *]

[a] *CAS Center for Excellence in Nanoscience, Beijing Key Laboratory of Micro-nano Energy and Sensor, Beijing Institute of Nanoenergy and Nanosystems, Chinese Academy of Sciences, Beijing 101400, China*

[b] *College of Engineering, Mathematics and Physical Sciences, University of Exeter, Exeter EX4 4QF, UK*

[c] *School of Nanoscience and Technology, University of Chinese Academy of Sciences, Beijing 100049, China*

[d] *Center on Nanoenergy Research, School of Physical Science and Technology, Guangxi University*

[e] *School of Mechanical Engineering, Xi'an Jiaotong University, Xi'an 710049, China;*

* Corresponding author at: *College of Engineering, Mathematics and Physical Sciences, University of Exeter (M. Zhu). Tribotronics Research Group, Beijing Institute of Nanoenergy and Nanosystems, Chinese Academy of Sciences (C. Zhang)*.

E-mail addresses: m.zhu@exeter.ac.uk (M. Zhu). czhang@binn.cas.cn (C. Zhang).

[1] These authors contributed equally to this work.

Abstract

Triboelectric Nanogenerators (TENGs) based on spring-assisted structures play a central role in scavenging vibrational energy that is widely available in the natural environment. However, they suffer from difficulties in adjusting the stiffness and bonding the springs to the triboelectric layer. Here, a kirigami-inspired TENG (KI-TENG) with a kirigami structure is demonstrated, which can be used as an ultra-wide-band vibrational energy harvester and self-powered acceleration sensor. The triboelectric layer of the KI-TENG can be easily processed into the kirigami structure with one or two-degree-of-freedom by laser cutting technology. The frequency responses of the KI-TENG under the influence of mass, acceleration, and initial distance are investigated in detail to optimize the structural design. With optimized structural parameters, the KI-TENG can not only harvest broadband vibration energy from 2 to 49 Hz in vertical vibration state but also obtain high output performance over a wide frequency range in horizontal vibration state. Moreover, the KI-TENG can be used as a sensor measuring acceleration from 1 to 9 m/s^2. This work demonstrates a compact TENG coupled with the kirigami structure for energy harvesting and active sensing, which has great prospects in intelligent plants, artificial intelligence, and the internet age.

KEYWORDS: Kirigami structure coupling, Vibrational energy harvester, Self-powered sensor, Ultra-wide-band, Triboelectric nanogenerator

1. Introduction

Micro-energies harvested from the ambient environment can act as a power source overcoming the limitations of traditional batteries or wired power supplies [1-4]. Vibrational energy has attracted significant attention as it is ubiquitous in daily lives in the form of human body motions, machine vibrations, structural strains, etc. [5-7]. It is appealing to harvest these energies as a potential power source for electronics. However, traditional vibrational energy harvesters based on electromagnetic [8], piezoelectric [9-13], and electrostatic [14] technologies show deficiencies such as complex structures, demanding materials, and extra power sources, which impede the further development of these harvesters. In addition, most harvesters can only have high power output under a narrow working bandwidth. The almost random, broadband, and small-amplitude nature of the vibrations in the environment makes conventional vibration energy harvesters ineffective in capturing this energy. Usually, there are two criteria to evaluate whether an energy harvester can effectively harvest vibrational energy [15, 16]. First of all, the harvester must have a broad working bandwidth so that it can harvest vibration energy in a broad frequency spectrum. Secondly, the harvester must have a high power output at low-frequency and small-amplitude vibrations, as the vibration frequencies presented in the ambient environment are mostly in the range of a few hertz to tens of hertz.

Triboelectric Nanogenerators (TENGs) based on contact electrification and electrostatic induction effects were invented in 2012 [17-20]. Since then, TENGs have been extensively researched to collect micromechanical energy from surroundings [21-24]. They have been proved to have enormous advantages such as simple structure [25, 26], wide range of materials [27, 28], light weight [29, 30], high efficiency at low frequencies and small amplitudes [31, 32], and natural broadband characteristics in contact separation mode [6, 33-37]. These features enable the TENGs to harvest vibrational energy more efficiently than conventional harvesters. Therein, the TENGs with spring-assisted structures demonstrate a tremendous potential in harvesting vibration energy at the wideband and small-amplitude conditions compared to those without springs [38-41]. The spring-assisted TENGs not only can transfer low frequency motion to high frequency but also can increase the process of charge accumulation to improve energy harvesting efficiency. What's more, the spring-assisted TENGs can both collect vibrational energy and act as an active sensor. Nonetheless, almost all aforementioned

TENGs consist of springs and stiff base material (e.g. acrylic, wood, and metal), which lead to drawbacks such as complicated fabrication of TENGs, hard-to-adjust stiffness, difficulty in bonding to the triboelectric layer, and the vibration monitoring can only perform in a narrow frequency range when used as the acceleration sensor. This impedes the further development of TENGs. As a result, a compact, springless, easy-to-process, and broadband TENG is extremely expected.

Here, a lightweight, easy-manufacturing, and low-cost kirigami-inspired TENG (KI-TENG) is demonstrated, which can be used as an ultra-wide-band vibrational energy collector and self-powered acceleration sensing element. The triboelectric layer of the KI-TENG can be easily processed into the kirigami structure with one or two-degree-of-freedom on a PET sheet by the precision laser fast cutting technology. The frequency responses of the KI-TENG under the influence of mass, acceleration, and initial distance are investigated in detail to optimize the structural design. Based on the optimized structural parameters, the KI-TENG not only can harvest broadband vibration energy from 2 to 49 Hz in the vertical vibration state but also obtain high output performance over a wide frequency range even in the horizontal vibration state. In addition, the KI-TENG can be used as an acceleration sensor, monitoring acceleration changes from 1 to 9 m/s^2. And, an acceleration monitoring circuit based on the KI-TENG is built to monitor the running state of the machine. This work demonstrates a compact TENG coupled with the kirigami structure for energy collecting and sensing, which has great prospects in intelligent plants, artificial intelligence, and the internet age.

2. Kirigami-inspired TENG and its working mechanism

Kirigami art can be used to conveniently manufacture various structures (Fig. 1a). The characteristics of the kirigami structures are dominated by the number and distribution of cuts, which can endow base materials with flexibility and deformability. Inspired by the kirigami art, a compact TENG coupled with a kirigami structure is designed, as shown in Fig. 1b. While the fabrication process is briefly demonstrated in the figure, the experimental section demonstrated the fabrication methods. The kirigami structure was fabricated from a polyethylene terephthalate (PET) sheet by precision laser fast scanning technology. The surface of the PET sheet was first segmented into different sections with a preset machining path by laser scanning in the vertical direction, as shown in Fig. 1b(i). After a repeated laser fast scanning process, the final morphology of the preset machining path was formed (Fig. 1b(ii)). Then, a copper film was stuck to the side of the kirigami structure as a friction material and electrode. Meanwhile, fluorinated ethylene propylene (FEP) was used as the other triboelectric material due to its prominent contact electrification property. The base and support parts were made of acrylic sheets, which have high mechanical strength and good machinability. A layer of the sponge was inserted between the FEP frication layer and the base to enhance the effective contact area. An ion etching was used to modify the surface of the FEP to further improve the friction surface charge. Fig. S1 showed the surface topography of the Cu and FEP friction layers observed by scanning electron microscopy (SEM). By integrating the kirigami structure, substrate, and friction layers, a compact and springless KI-TENG was formed, as shown in Fig. 1b(iii-iv).

The working mechanism of the KI-TENG on account of the contact-separation mode is illustrated in Fig. 1c. At the initial state (Fig. 1c(i)), the FEP friction layer and Cu friction layer are completely contacted. The electrons will move from the surface of the Cu film to that of the FEP film, according to the triboelectric series. The surfaces of the FEP film and the Cu film acquire equal and opposite charges. In this stage, the KI-TENG can obtain a state of electrostatic equilibrium and there is no electron flow in the external circuit. When the KI-TENG is actuated by external vibration, the Cu film is separated from the FEP film (Fig. 1c(ii)) and a potential difference is produced between the two friction layers. The potential difference drives the electrons to flow from the FEP friction layer to the Cu friction layer through the external circuit to obtain an electrostatic balance. The electron transfer

process continues until the maximum distance between the Cu and FEP friction layers is reached, during which all the electrons will be moved to the Cu friction layer (Fig. 1c(iii)). Following the maximum distance is reached, the Cu friction layer moves downwards, and the distance between the two friction layers decreases (Fig. 1c(iv)). The electrons flow from the Cu friction layer back to the FEP friction layer to re-establish an electrostatic equilibrium, producing a reverse current. When the Cu film is completely in contact with the FEP film again, all the electrons can flow back to the FEP friction layer and the electrostatic equilibrium is regained. This is the entire process of electron transfer between Cu and FEP friction layers, which continuously generates pulsed currents, thus converting mechanical energy into electrical energy.

3. Experimental section

3.1. Fabrication of the KI-TENG

A commercial software AutoCAD 2022 was utilized to design the kirigami structure of the KI-TENG. Then, the patterned structure is imported into the precision laser fast scanning laser (D90M). After that, the kirigami structure with one or two-degree-of-freedom on the PET sheet was processed according to the preset processing path. A Cu film was attached to the kirigami structure as the triboelectric layer, which had a thickness and diameter of 65 μm and 26 mm, respectively. The acrylic was cut by a precision laser fast scanning laser, which was used as the base and had a diameter of 86 mm. Then a sponge layer (3 mm thick), a Cu film (65 μm thick), and a FEP film (12 μm thick) were sequentially attached to the center of the acrylic and all of them had the same diameter of 26 mm.

3.2. Fabrication of the micro-nano structures on FEP surface

The FEP film was etched by an inductively coupled plasma (ICP) to form the micro-nano structures. First, the gold spray coater (108Auto) was used to deposit gold particles on the surface of the FEP film with a spray time of 15s. Gold particles as the mask can protect the surface of FEP during the etching process to form micro-nano structures. In addition, there is no specific requirement for the metal nanoparticles of the mask, which can be gold, copper, silver, etc. nanoparticles [42, 43]. Then, the gold-based FEP film was placed in the ICP equipment at a gas flow rate of 10, 20, and 30 sccm for oxygen, argon, and carbon tetrafluoride respectively. The plasma was generated by a power source of 400 W. And another power source of 100W was used to accelerate the plasma. Finally, the gold-based FEP film was etched for 120s to get micro-nano structures.

3.3. Electric measurement and characterization

The surface morphologies of the FEP and Cu film were measured by a cold field emission scanning electron microscope (SU8020). The surface microstructure of FEP was manufactured by the ICP etching instrument (SENTECH SI 500). The external excitation was supplied by a small vibrating device (KSI-758ST500), which also included a power amplifier unit (KSI-758PA800) and a control unit (VT-9002). The voltage, charge, and current of the KI-TENG were tested by an electrometer (Keithley 6514). Furthermore, the real-time data was recorded by the software platform LabVIEW.

4. Results and discussions

4.1. Parametric study of KI-TENG with single-degree-of-freedom kirigami structure

A KI-TENG with a single-degree-of-freedom kirigami structure (Fig. 2a) was first considered in this study. Fig. 2b illustrates the structure of KI-TENG. The dynamics of the KI-TENG can be described by Eqs. (1-2).

$$m_1\ddot{y}_1 + c_1\dot{y}_1 + k_1y_1 - F_e = -m\ddot{y}_0,\ (y_1 > -d) \tag{1}$$

$$m_1\ddot{y}_1 + (c_0 + c_1)\dot{y}_1 + (k_1 + k_0)y_1 + k_0d = -m\ddot{y}_0,\ (y_1 \leq -d) \tag{2}$$

where $y_0(t) = Y\,sin(\omega t)$ with Y being the amplitude and ω the angular frequency of the actuation displacement, y_1 is the relative motion to the basement, F_e is the electrostatic force. The average method can be used to solve the Eqs. (1) and (2), which is demonstrated in the Supporting Note S1 of Supporting Information. In this model, certain parameters such as acceleration, stiffness, mass, and the gap distance show strong influences on the amplitude-frequency characteristics of KI-TENG with single-degree-of- freedom. Among the above parameters, the acceleration range will greatly affect the amplitude of KI-TENG, while the stiffness and mass variation will affect the resonance point of KI-TENG. The change in the gap distance will affect the output of KI-TENG. In this work, we aim to design structures to explore the location of resonance points of single-degree-of-freedom KI-TENG for better energy harvesting in practical vibration scenarios. And the stiffness k_0 generated during the collision does not affect the position of the resonance peak, so the stiffness and damping in the collision was neglected. According to the above analysis, assume that the initial values of mass m_1, acceleration, and stiffness k_1 are 20 g, 3 m/s^2, and 1300 N/m, respectively. The vibration amplitude of KI-TENG with single-degree-of-freedom could be simulated, as shown in Fig. S2. The results suggest that the increase of external excitation does not change the location of its resonance point, but affects its vibration amplitude; the greater the excitation, the greater the amplitude. In addition, the stiffness change will mainly affect the location of its vibration frequency point. Then, the frequency responses of the KI-TENG were measured in the experimental, and a test setup was built, as shown in Fig. 2c. It consists of a data acquisition and vibration control system, an acceleration sensor, a shaker, and the KI-TENG. Using this experimental setup, the effects of the acceleration (a), initial mass (m_1), initial distance (d), and stiffness (k_1) of the kirigami structure are investigated in detail.

Thereof, the elements affecting the stiffness k_1 mainly include the length, width, and the number of the beams in the kirigami structure. When one parameter was studied, the others were kept constant. Unless specified otherwise, the acceleration, mass and initial distance were 3 m/s^2, 20 g, and 0.3 mm, respectively while the number, length, and width of the beams of were 3, 10 mm, and 1.5 mm, respectively.

Fig. 2d-f shows the influences of the acceleration, initial distance, and mass on the frequency response of the KI-TENG. As the excitation acceleration varied from 1 to 5 m/s^2, the electrical output and the frequency band become larger (Fig. 2d). The reason is that the increase in acceleration leads to the raise in the available touch region between the two friction layers over a wider frequency range, thereby increasing their electrical output and frequency band. This is the same as the variation law of the amplitude frequency effect of acceleration on KI-TENG in the simulation. In addition, acceleration is not a parameter that can be optimised. Instead, it is a condition which varies widely in reality. In this study, when the acceleration reaches 3 m/s^2 or beyond, the energy harvester has demonstrated full output characteristics. Although further increase in the acceleration undoubtedly will increase the bandwidth and voltage output, an acceleration of 3 m/s^2 is sufficient to demonstrate the characteristics of the energy harvester. The mass has a significant impact on the frequency band of KI-TENG (Fig. 2e). As the mass is increased from 1 to 20 g, the peak voltage increases from nearly zero to 39 V, along with a rapidly increased frequency bandwidth. The voltage output with a mass of 1 g is close to zero. This is probably because the mass is too small to allow contact separation of the two friction layers. It can also be observed that increasing the mass can shift the intrinsic frequency of the KI-TENG to a lower frequency. Fig. 2f presents the effect of initial distance on the frequency and electric response of KI-TENG. As the distance between the two friction layers is decreased, both the working bandwidth and the output voltage go up. This is because with a smaller initial distance, the Cu friction layer impacts the EFP layer at a higher velocity, leading to a larger contacting force and a larger contact area.

These are the effects of external factors on the frequency response of KI-TENG, while the kirigami structure also has an important effect on the frequency response. The beam width was first explored, as shown in Fig. 2g. As the beam width increases, the frequency band of the KI-TENG

becomes narrower. The reason is that a wider beam leads to a higher stiffness constant, giving rise to less elastic deformation and thus a lower working bandwidth. As a result, the beam width is set to 1.5 mm in this paper. Fig. 2h illustrates the effect of the beam length on the frequency response of KI-TENG. The increase in the beam length produces a significant improvement in the working bandwidth. However, an increased beam length can bring about a rapid increase in the volume of the TENG. So, the spring length is set to 10 mm in this paper. The effect of the beam number was also studied in detail (Fig. 2i). These experimental results suggest as the beam number raises, the bandwidth of the KI-TENG first increases and then decreases. The maximum output voltage and bandwidth are obtained with 3 beams. Therefore, the beam number is set to 3.

4.2. Electrical characteristics of KI-TENG with two-degree-of-freedom kirigami structure

To further improve the bandwidth of the KI-TENG, a kirigami structure with two degrees of freedom, as shown in Fig. 3a, was designed and studied. The additional degree of freedom is represented by a mass m_2, stiffness k_2 and damping coefficient c_2 in Fig. 3b. The corresponding nonlinear equation of amplitude-frequency response of KI-TENG based on the mechanical model can be given by:

$$\begin{cases} m_1(\ddot{y}_1 + \ddot{y}_0) + c_1\dot{y}_1 + k_1y_1 - c_2\dot{y}_2 - k_2y_2 + f(\dot{y}_1, y_1) = 0 \\ m_2(\ddot{y}_2 + \ddot{y}_1 + \ddot{y}_0) + c_2\dot{y}_2 + k_2y_2 = 0 \end{cases} \tag{3}$$

$$f(\dot{y}_1, y_1) = \begin{cases} -F_e, (y_1 \geq -d) \\ c_0\dot{y}_1 + k_0(y_1 + d), (y_1 < -d) \end{cases} \tag{4}$$

Where y_2 is the relative motion to the y_1. The derivation of the Eqs. (3) and (4) are demonstrated in the Supporting Note S2 of Supporting Information. In this model, the acceleration, stiffness, mass, and the gap distance also strongly influence on the amplitude-frequency characteristics of KI-TENG with two-degree-of-freedom. Based on the analysis of the single-degree-of-freedom system, the influence of stiffness and acceleration changes on the amplitude-frequency characteristics of KI-TENG is also mainly analyzed in the two-degree-of-freedom system. Here, assume that the initial values of mass m_2, acceleration, and stiffness k_2 are 80 g, 3 m/s^2, and 200 N/m, respectively. Then, the vibration amplitude of KI-TENG with two-degree-of-freedom was simulated, as shown in Fig. S3. The results suggest that different parameters will affect the position of the two peaks in the two-degree-of-freedom system. In addition, according to the KI-TENG with single-degree-of-freedom kirigami structure

parametric study, increasing the mass may shift the intrinsic frequency of the KI-TENG to the left. After increasing the mass to 80 g, the frequency band characteristics of KI-TENG were explored, as shown in Fig. S4. The experimental results show that the increase of mass can make a large left shift in the frequency band of KI-TENG. The initial value of m_2 was slso determined. As a result, based on the parametric study of the single-degree-of-freedom KI-TENG, the acceleration, the mass of m_2 and initial distance were 3 m/s^2, 80 g, and 0.3 mm, respectively while the number, length, and width of the beams of were 3, 10 mm, and 1.5 mm, respectively. The KI-TENG with two degrees of freedom shows two resonance peaks as shown in Fig. 3c. Furthermore, the related properties of the spring have been studied in detail, so only the influences of the acceleration, initial distance, and mass changes on the KI-TENG working bandwidth with two degrees of freedom are investigated (Fig. 3d-f).

Fig. 3d shows the effect of acceleration variation on the frequency band of KI-TENG. As the excitation acceleration varied from 1 to 5 m/s^2, both the working bandwidth and electric output increased. This is the same as the effect of acceleration on the frequency response of KI-TENG with single-degree-of-freedom. When the initial distance between the two friction layers is enlarged, the working bandwidth becomes smaller, as shown in Fig. 3e. This is because the increase of the initial distance will make the friction layers contact only in a narrow frequency range. In addition, the mass m_2 also shows a significant impact on the frequency band of KI-TENG (Fig. 3f). As the mass is varied from 40 to 120 g, the working bandwidth and electric output increase while the resonance of the KI-TENG shifts to a lower frequency. The outcomes indicate that increasing acceleration, reducing gap distance, and increasing mass can broaden the working bandwidth of the KI-TENG. Therefore, choosing the appropriate parameters to manufacture the KI-TENG with two-degree-of-freedom can scavenge environmental vibration energy in a broad frequency spectrum. Based on the results in Fig. 2 and 3, the KI-TENG was optimised with a mass of 100 grams and an initial distance of 0.1 mm. Further reducing the initial distance was found to lead to difficulties in the separation of the two friction layers when actuated due to the electrostatic force. In addition, the mass of m_1 is 20 g and the mass of m_2 is 80 g. Then, the open-circuit voltage of the optimised KI-TENG actuated at 5 m/s^2 was measured, as shown in Fig. 3g. The corresponding transferred charge and vibration amplitude of KI-TENG were also tested and presented in Figs. S5 and S6, respectively. Therein, the vibration amplitude

of KI-TENG was measured by a laser displacement sensor (HL-G103-A-C5) . The results suggest that when the initial distance is set to 0.1 mm, the KI-TENG can produce a large output whenever the vibration amplitude is greater than 0.1 mm. In addition, to further investigate whether the KI-TENG can effectively harvest wideband vibration energy when it is at different angles from the horizontal surface, we have conducted relevant experimental demonstrations, as shown in Fig. S7. The experimental results show that KI-TENG can keep the working bandwidth and output almost constant even at an inclination angle of 30 degrees. As the vibration tilt angle increases to 45 degrees, the bandwidth remains above 30 Hz. When the vibration changes completely from vertical to horizontal, the KI-TENG still maintains good output characteristics in the 2 to 14 Hz frequency vibration range. This shows that the KI-TENG can be used as a wideband vibration energy harvester even when the vertical vibration component is zero. As a result, the optimised KI-TENG could always get good electric characteristics over a broad frequency scope from 2 to 49 Hz. In addition, the durability of KI-TENG was tested, as shown in Fig. S8. After 50,000 cycles at 15 Hz, the output of the KI-TENG remained almost constant, demonstrating its excellent stability. So far, several methods such as parameter optimization [6], resonant design [34], and structural integration [26] have been used to improve the working bandwidth of TENGs. With these methods, the working bandwidth of the TENG has been increased from 11.2 to 42 Hz, as shown in Fig. 3h. In comparison, the KI-TENG with a kirigami structure demonstrates an ultra-wide working bandwidth of 47 Hz.

Based on the above theoretical analysis and experimental research, the design criteria of KI-TENG can be concluded. First, the application scenario of KI-TENG needs to be determined so that the frequency range and acceleration of the environmental vibration can be obtained. Then, choose the mass and stiffness of KI-TENG. The pre-selected values of the mass and stiffness can be determined by simulation. The selection principle follows that increasing the mass will make the resonance point decrease, and increasing the stiffness will increase the resonance point. Afterward, the number, length, and width of KI-TENG beams are adjusted to determine the stiffness and the range of resonance points. The gap value determines the size of the frequency band; the smaller the gap distance, the wider the frequency band. However, the gap value is too small and may be affected by electrostatic adsorption. Therefore, the gap value is chosen reasonably according to the environmental vibration.

Finally, kirigami structures with one or two-degree-of-freedom can be prepared by using precision laser processing.

4.3. Potential application of the KI-TENG

Such a KI-TENG with ultra-wide working bandwidth has a wide range of promising applications in various vibration environments like engines, trains, gear and belt drive systems, airplanes, and automobiles (Fig. 4a). As shown in Supplementary Videos S1 and S2, KI-TENG has proven to be effective in harvesting the vibration energy generated by vacuum pumps and automobiles engines. The KI-TENG can not only scavenge these vibration energies to power various electronics but also serve as self-powered sensors. Fig. 4b shows the electric output of the KI-TENG when the acceleration and frequency are changed. Fig. S9 shows the detailed variation curves of the voltage of the KI-TENG. The results suggest that the KI-TENG has a good acceleration monitoring performance and can measure acceleration from 1 to 9 m/s^2 over a frequency range from10 to 20 Hz. In addition, the KI-TENG shows a good linearity in the acceleration range of 1–5 m/s^2 and 5.5-9 m/s^2 at 15 Hz with a sensitivity of about 3.6 $V/(m/s^2)$ and 17.5 $V/(m/s^2)$, respectively, as shown in Fig. S10. To further demonstrate its capability of working as a self-powered acceleration sensor to check the running state of the machine, an acceleration monitoring circuit was built, which consisted of a self-powered charging unit and an equipment malfunction alarm unit, as shown in Fig. 4c. The self-powered charging unit comprised of a rectifier and a storage capacitor (C_s) converts the alternating current (AC) signal generated to a direct current (DC) signal and stores it in C_s. The equipment malfunction alarm unit consists of resistors (R_1, R_2), a Zener diode (D), and a MOSFET, which can monitor the running state of the machine. When the voltage of C_s is more than the threshold voltage of the MOSFET, the electronic switch is turned on. Then, the load works to simulate an equipment malfunction alarm. Thereof, the electrical energy can be released from the C_s by the R_1 to guard against the system from being triggered in error. The Zener diode D and resistor R_2 are used to protect the MOSFET and the load, respectively.

The influences of the capacitance of C_s and the resistance of R_1 on the voltage of C_s were investigated, as shown in Fig. 4d and 4e. The acceleration and the frequency were set as 5 m/s^2 and 15 Hz, respectively. Fig. 4d illustrates the voltage output responses of C_s with different capacitances. As

the MOSFET threshold voltage was adjusted to 2.5 V, the response process of the system was the time of voltage of the C_s changed from 0 to 2.5 V. In addition, experimental results suggest that the capacitance value of C_s is inversely proportional to the system response time. A smaller capacitor may reduce the response time but will make the load circuit unstable. As a result, the capacitance value of 220 nF was chosen. Fig. 4e shows the voltage output response of C_s with different resistances, which indicates that the voltage value of C_s increases with increasing resistance. Therefore, when the capacitance value is constant, the working state of MOSFET can be controlled by changing the magnitude of the resistance value. Fig. 4f and Supplementary Video S3 present an intuitive visual representation of KI-TENG as a self-powered acceleration sensor. The load here was represented by a LED. When the acceleration was less than 5 m/s^2, the MOSFET was not turned on, so the LED was not energized. The MOSFET was turned on and the LED was illuminated when the acceleration was more than 5 m/s^2. This demonstrates an important application of KI-TENG as a self-powered acceleration sensor for equipment malfunction alarms.

5. Conclusion

In summary, a kirigami-inspired TENG is demonstrated, which has a compact, springless, easy-to-process structure and can be used as an ultra-wide-band vibrational energy harvester and self-powered acceleration sensor. Thereof, the friction layer of the KI-TENG can be easily processed into the kirigami structure with one or two degrees of freedom on a PET sheet by the precision laser fast cutting technology. Then, the dependence of the frequency response characteristics of the KI-TENG on mass, acceleration, and initial distance are investigated in detail to optimize its structural design. Experimental results suggest that the KI-TENG will achieve a broader working bandwidth under a larger acceleration and a smaller distance. Moreover, increasing the quality will change the frequency response to a lower frequency, meanwhile expanding the frequency band characteristics in part. Based on the optimized structural parameters, the KI-TENG can not only incessantly harvest broadband vibration energy from 2 to 49 Hz in the vertical vibration state but also obtain high output performance over a wide frequency range even in the left-right vibration state. In addition, the KI-TENG can be used as an acceleration sensor with a measurement range from 1 to 9 m/s^2. An acceleration monitoring circuit based on the KI-TENG was built to monitor the running state of the machine. This work demonstrates a compact TENG coupled with the kirigami structure for energy harvesting and active sensing, which has great prospects in intelligent plants, artificial intelligence, and the internet age.

Declaration of Competing Interest

The authors declare that they have no known competing financial interests or personal relationships that could have appeared to influence the work reported in this paper.

Acknowledgments

This research was supported by the National Natural Science Foundation of China (Nos. 51922023, 61874011), and Fundamental Research Funds for the Central Universities (E1EG6804).

Appendix A. Supplementary material

Supplementary data to this article can be found online at https://doi.*****

CRediT authorship contribution statement

Youchao Qi: Investigation, Experimentation, Writing-original draft. **Yang Kuang:** Conceptualization, Writing-original draft. **Yaoyao Liu:** Conceptualization, Investigation. **Guoxu Liu:** Investigation, Validation. **Jianhua Zeng:** Validation. **Junqing Zhao:** Investigation. **Lu Wang:** Validation. **Meiling Zhu:** Conceptualization, Supervision, Writing-review & editing. **Chi Zhang:** Conceptualization, Resources, Supervision, Writing-review & editing.

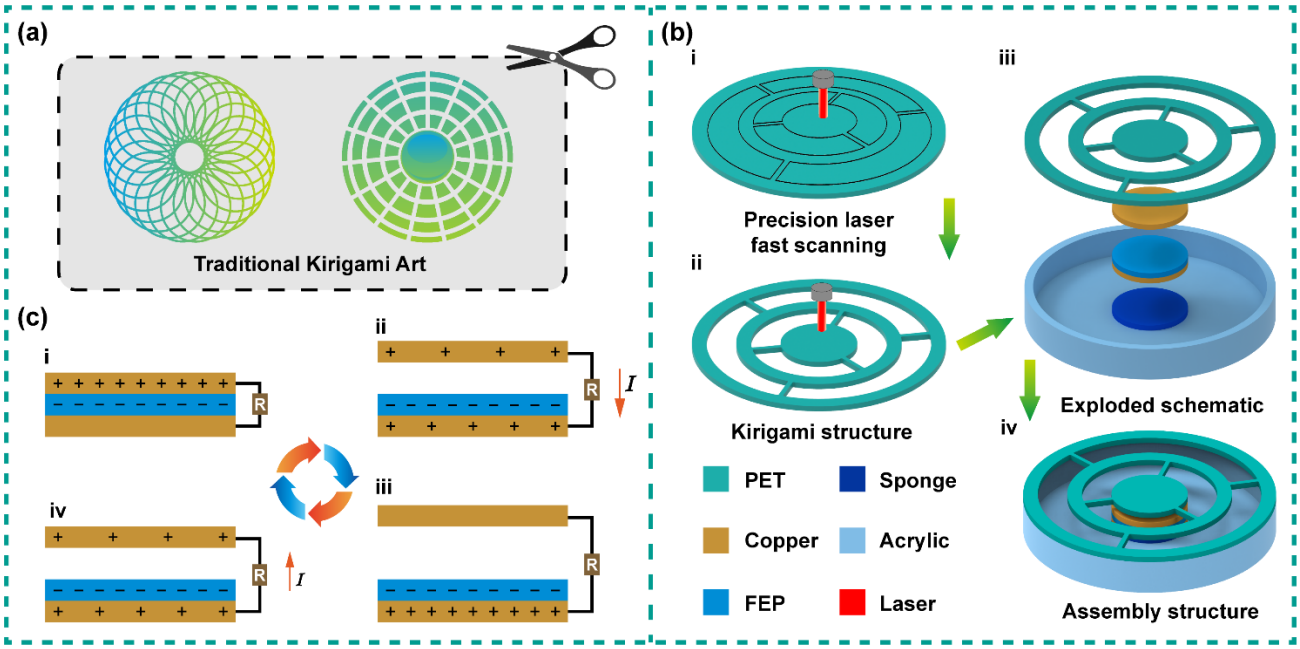

Fig. 1. The fabrication process, kirigami structure design, and working mechanism of a kirigami-inspired triboelectric nanogenerator (KI-TENG). (a) Various artistic shapes made by kirigami art. (b) Precision laser fast scanning processes for preparing kirigami structure on a sheet of PET. (c) The working process of the KI-TENG.

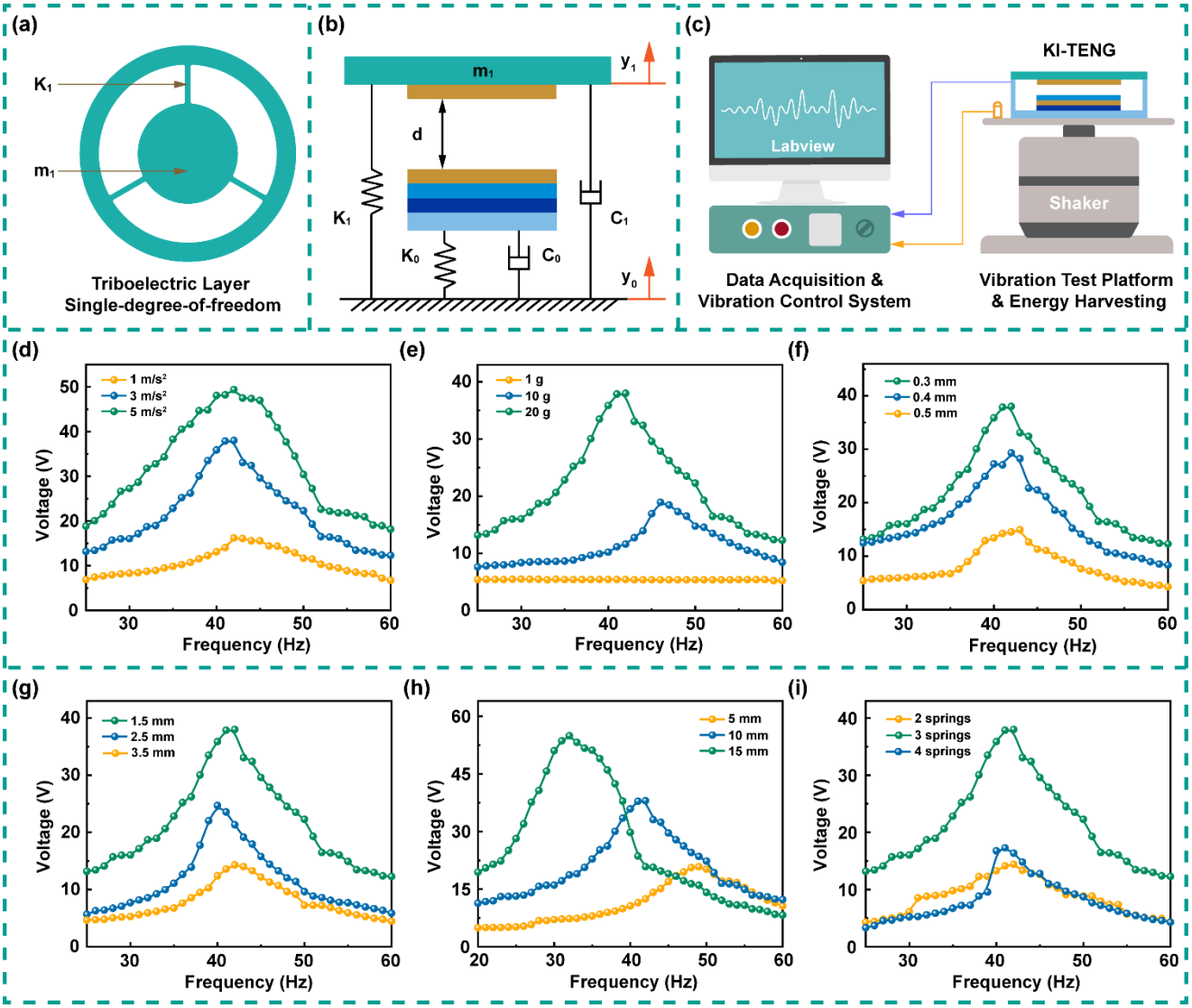

Fig. 2. Experimental setup, the electric characteristics of the KI-TENG with various structural parameter factors. (a) Structural parameter of the KI-TENG with the single-degree-of-freedom condition. (b) The mechanical model of the KI-TENG with single-degree-of-freedom. (c) Vibration testing setup for energy harvesting and data acquisition. The influence of different excitation accelerations (d), moving masses (e), initial distances (f), the widths (g), lengths (h), and the number (i) of the beam in the kirigami structure on output response characteristics of the KI-TENG.

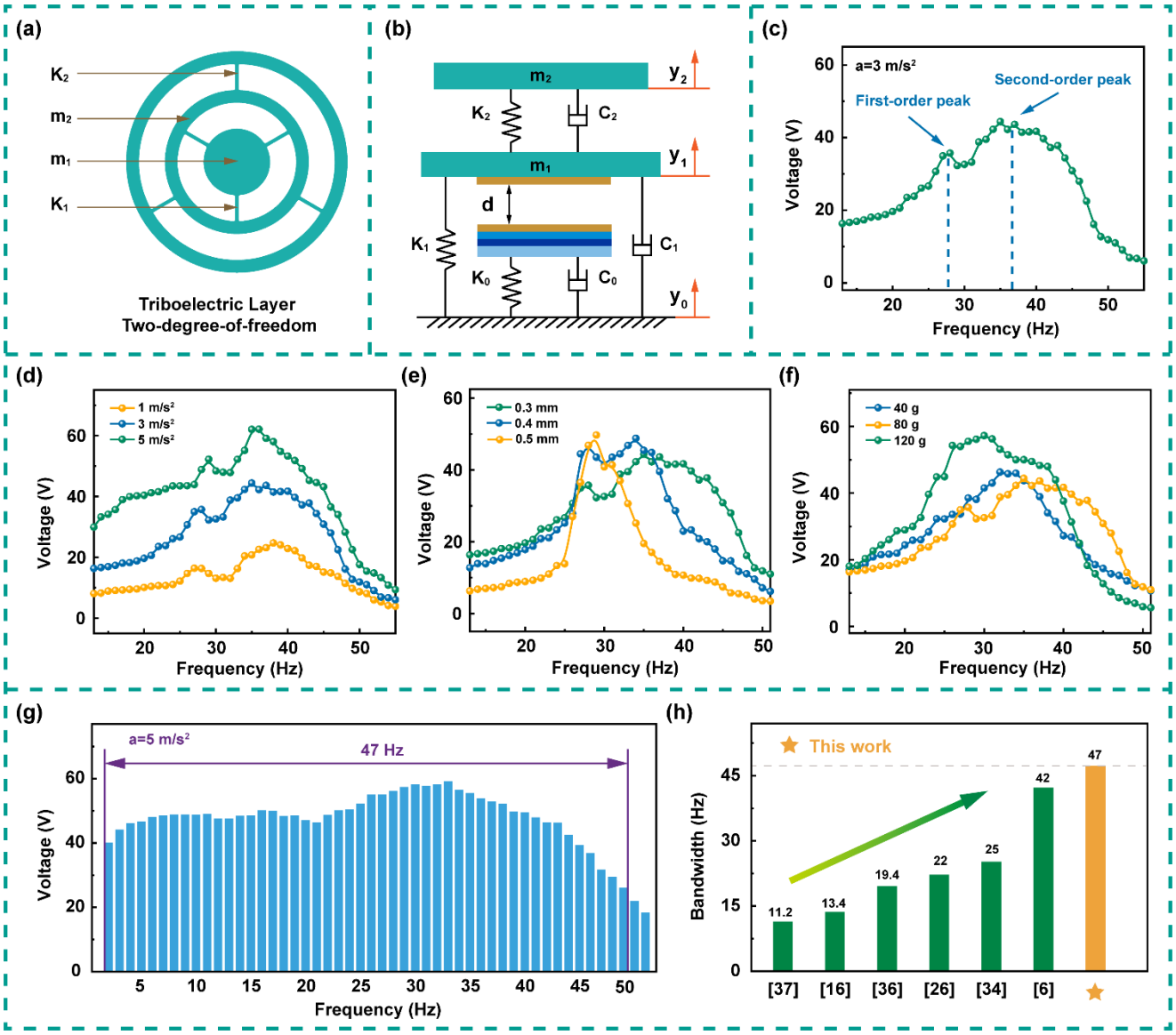

Fig. 3. Electric output response of the KI-TENG with a two-degree-of-freedom structure. (a) Structural parameter of the KI-TENG with the two-degree-of-freedom condition. (b) The mechanical model of the KI-TENG with two-degree-of-freedom. (c) The KI-TENG can obtain two resonance peaks. The influence of different excitation accelerations (d), initial distances (e), and moving masses (f) on output response characteristics of the KI-TENG. (g) The voltage characteristics of KI-TENG at the acceleration of 5 m/s^2. (h) Comparison of the bandwidth of various vibration energy harvesters with KI-TENG.

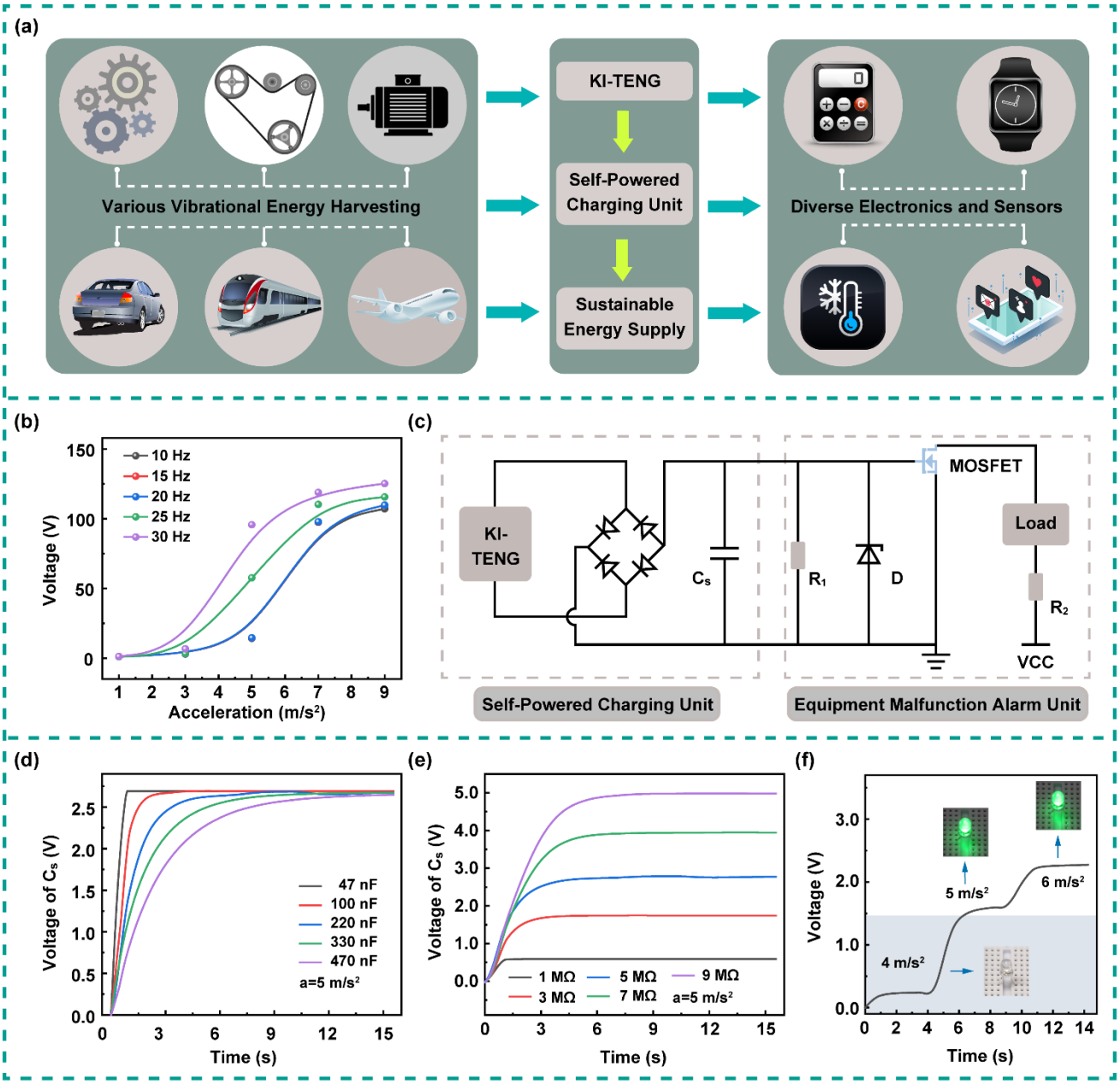

Fig. 4. Demonstrations of the ultra-wide-band KI-TENG as a self-powered acceleration sensor, equipment malfunction alarm, and potential application. (a) Extension of the KI-TENG for energy harvesting and sensing applications. (b) KI-TENG can be used as a self-powered accelerometer to monitor acceleration changes in a broad frequency range from 10 to 20 Hz. (c) The equipment malfunction alarm circuit using KI-TENG. (d) The voltage of the C_s with different capacitance (d) and different resistance (e) at excitation acceleration of 5 m/s^2, respectively. (f) The voltage changes at the different excitation accelerations.

References

[1] Hittinger E, Jaramillo P. Internet of Things: Energy boon or bane? Science 2019;364(6438):326-328.

[2] Long L, Liu W, Wang Z, He W, Li G, Tang Q, et al. High performance floating self-excited sliding triboelectric nanogenerator for micro mechanical energy harvesting. Nat. Commun. 2021;12(1):4689.

[3] Li X, Cao Y, Yu X, Xu Y, Yang Y, Liu S, et al. Breeze-driven triboelectric nanogenerator for wind energy harvesting and application in smart agriculture. Appl. Energy 2022;306.

[4] Sun R, Li Q, Yao J, Scarpa F, Rossiter J. Tunable, multi-modal, and multi-directional vibration energy harvester based on three-dimensional architected metastructures. Appl. Energy 2020;264.

[5] He J, Fan X, Zhao D, Cui M, Han B, Hou X, et al. A high-efficient triboelectric-electromagnetic hybrid nanogenerator for vibration energy harvesting and wireless monitoring. Sci. China-Inf. Sci. 2021;65(4):142401.

[6] Qi Y, Liu G, Gao Y, Bu T, Zhang X, Xu C, et al. Frequency Band Characteristics of a Triboelectric Nanogenerator and Ultra-Wide-Band Vibrational Energy Harvesting. ACS Appl. Mater. Interfaces 2021;13(22):26084-26092.

[7] Chen J, Wang Z L. Reviving Vibration Energy Harvesting and Self-Powered Sensing by a Triboelectric Nanogenerator. Joule 2017;1(3):480-521.

[8] Dong L, Closson A B, Jin C, Trase I, Chen Z, Zhang J X J. Vibration-Energy-Harvesting System: Transduction Mechanisms, Frequency Tuning Techniques, and Biomechanical Applications. Adv. Mater. Technol. 2019;4(10):1900177.

[9] Liu H, Lee C, Kobayashi T, Tay C J, Quan C. Investigation of a MEMS piezoelectric energy harvester system with a frequency-widened-bandwidth mechanism introduced by mechanical stoppers. Smart Mater. Struct. 2012;21(3):035005.

[10] Safaei M, Sodano H A, Anton S R. A review of energy harvesting using piezoelectric materials: state-of-the-art a decade later (2008–2018). Smart Mater. Struct. 2019;28(11):113001.

[11] Kuang Y, Chew Z J, Dunville J, Sibson J, Zhu M. Strongly coupled piezoelectric energy harvesters: Optimised design with over 100 mW power, high durability and robustness for self-powered condition monitoring. Energy Conv. Manag. 2021;237:114129.

[12] Qi N, Dai K, Wang X, You Z. Optimization for piezoelectric energy harvesters with self-coupled structure: A double kill in bandwidth and power. Nano Energy 2022;102:107602.
[13] Seol M-L, Im H, Moon D-I, Woo J-H, Kim D, Choi S-J, et al. Design Strategy for a Piezoelectric Nanogenerator with a Well-Ordered Nanoshell Array. ACS Nano 2013;7(12):10773-10779.
[14] Khan F U, Qadir M U. State-of-the-art in vibration-based electrostatic energy harvesting. J. Micromech. Microeng. 2016;26(10):103001.
[15] Kulah H, Najafi K. Energy Scavenging From Low-Frequency Vibrations by Using Frequency Up-Conversion for Wireless Sensor Applications. IEEE Sens. J. 2008;8(3):261-268.
[16] Chen J, Zhu G, Yang W, Jing Q, Bai P, Yang Y, et al. Harmonic-Resonator-Based Triboelectric Nanogenerator as a Sustainable Power Source and a Self-Powered Active Vibration Sensor. Adv. Mater. 2013;25(42):6094-6099.
[17] Fan F-R, Tian Z-Q, Wang Z L. Flexible triboelectric generator. Nano Energy 2012;1(2):328-334.
[18] Wang Z L, Wang A C. On the origin of contact-electrification. Mater. Today 2019;30:34-51.
[19] Wang S, Lin L, Wang Z L. Nanoscale Triboelectric-Effect-Enabled Energy Conversion for Sustainably Powering Portable Electronics. Nano Lett. 2012;12(12):6339-6346.
[20] Shao J, Yang Y, Yang O, Wang J, Willatzen M, Wang Z L. Designing Rules and Optimization of Triboelectric Nanogenerator Arrays. Adv. Energy Mater. 2021;11(16):2100065.
[21] Chen G, Li Y, Bick M, Chen J. Smart Textiles for Electricity Generation. Chem. Rev. 2020;120(8):3668-3720.
[22] Zhang S, Bick M, Xiao X, Chen G, Nashalian A, Chen J. Leveraging triboelectric nanogenerators for bioengineering. Matter 2021;4(3):845-887.
[23] Zhao X, Askari H, Chen J. Nanogenerators for smart cities in the era of 5G and Internet of Things. Joule 2021;5(6):1391-1431.
[24] Zou Y, Xu J, Fang Y, Zhao X, Zhou Y, Chen J. A hand-driven portable triboelectric nanogenerator using whirligig spinning dynamics. Nano Energy 2021;83:105845.
[25] Wang L, He T, Zhang Z, Zhao L, Lee C, Luo G, et al. Self-sustained autonomous wireless sensing based on a hybridized TENG and PEG vibration mechanism. Nano Energy 2021;80:105555.
[26] Wang X, Niu S, Yi F, Yin Y, Hao C, Dai K, et al. Harvesting Ambient Vibration Energy over a

Wide Frequency Range for Self-Powered Electronics. ACS Nano 2017;11(2):1728-1735.
[27] Tang W, Jiang T, Fan F R, Yu A F, Zhang C, Cao X, et al. Liquid-Metal Electrode for High-Performance Triboelectric Nanogenerator at an Instantaneous Energy Conversion Efficiency of 70.6%. Adv. Funct. Mater. 2015;25(24):3718-3725.
[28] Pu X, Liu M, Li L, Han S, Li X, Jiang C, et al. Wearable Textile-Based In-Plane Microsupercapacitors. Adv. Energy Mater. 2016;6(24):1601254.
[29] Xu Z, Li D, Wang K, Liu Y, Wang J, Qiu Z, et al. Stomatopod-inspired integrate-and-fire triboelectric nanogenerator for harvesting mechanical energy with ultralow vibration speed. Appl. Energy 2022;312:118739.
[30] Kong D S, Han J Y, Ko Y J, Park S H, Lee M, Jung J H. A Highly Efficient and Durable Kirigami Triboelectric Nanogenerator for Rotational Energy Harvesting. Energies 2021;14(4):1120.
[31] Zhao J, Zhen G, Liu G, Bu T, Liu W, Fu X, et al. Remarkable merits of triboelectric nanogenerator than electromagnetic generator for harvesting small-amplitude mechanical energy. Nano Energy 2019;61:111-118.
[32] Xu S, Fu X, Liu G, Tong T, Bu T, Wang Z L, et al. Comparison of applied torque and energy conversion efficiency between rotational triboelectric nanogenerator and electromagnetic generator. iScience 2021;24(4):102318.
[33] Yang J, Chen J, Yang Y, Zhang H, Yang W, Bai P, et al. Broadband Vibrational Energy Harvesting Based on a Triboelectric Nanogenerator. Adv. Energy Mater. 2014;4(6):1301322.
[34] Bhatia D, Kim W, Lee S, Kim S W, Choi D. Tandem triboelectric nanogenerators for optimally scavenging mechanical energy with broadband vibration frequencies. Nano Energy 2017;33:515-521.
[35] Ibrahim A, Ramini A, Towfighian S. Experimental and theoretical investigation of an impact vibration harvester with triboelectric transduction. J. Sound Vibr. 2018;416:111-124.
[36] Salauddin M, Toyabur R M, Maharjan P, Rasel M S, Cho H, Park J Y. Design and experimental analysis of a low-frequency resonant hybridized nanogenerator with a wide bandwidth and high output power density. Nano Energy 2019;66:104122.
[37] Zhang L, Jin L, Zhang B, Deng W, Pan H, Tang J, et al. Multifunctional triboelectric nanogenerator based on porous micro-nickel foam to harvest mechanical energy. Nano Energy

2015;16:516-523.

[38] Xu M, Wang P, Wang Y-C, Zhang S L, Wang A C, Zhang C, et al. A Soft and Robust Spring Based Triboelectric Nanogenerator for Harvesting Arbitrary Directional Vibration Energy and Self-Powered Vibration Sensing. Adv. Energy Mater. 2018;8(9):1702432.

[39] Gupta R K, Shi Q, Dhakar L, Wang T, Heng C H, Lee C. Broadband Energy Harvester Using Non-linear Polymer Spring and Electromagnetic/Triboelectric Hybrid Mechanism. Sci Rep 2017;7(1):41396.

[40] Wu C, Liu R, Wang J, Zi Y, Lin L, Wang Z L. A spring-based resonance coupling for hugely enhancing the performance of triboelectric nanogenerators for harvesting low-frequency vibration energy. Nano Energy 2017;32:287-293.

[41] Hu Y, Yang J, Jing Q, Niu S, Wu W, Wang Z L. Triboelectric Nanogenerator Built on Suspended 3D Spiral Structure as Vibration and Positioning Sensor and Wave Energy Harvester. ACS Nano 2013;7(11):10424-10432.

[42] Pang Y K, Li X H, Chen M X, Han C B, Zhang C, Wang Z L. Triboelectric Nanogenerators as a Self-Powered 3D Acceleration Sensor. ACS Appl. Mater. Interfaces 2015;7(34):19076-19082.

[43] Xu L, Bu T Z, Yang X D, Zhang C, Wang Z L. Ultrahigh charge density realized by charge pumping at ambient conditions for triboelectric nanogenerators. Nano Energy 2018;49:625-633.